A Phase-Behavior Study for *n*-Hexane/Bitumen and *n*-Octane/Bitumen Mixtures

Jianyi Gao, University of Alberta; **Ryosuke Okuno,** University of Texas at Austin; and **Huazhou Andy Li,** University of Alberta

Summary

Steam/solvent coinjection has been studied as a potential method to improve the efficiency of conventional steam-assisted gravity drainage (SAGD) for bitumen recovery. This research is part of an experimental program for phase behavior of Athabasca-bitumen/solvent mixtures.

This paper presents a new set of experimental data for phase equilibrium, viscosity, density, and asphaltene precipitation for 11 mixtures of Athabasca bitumen with *n*-hexane and 10 mixtures of the same bitumen with *n*-octane. Phase-boundary measurements were conducted at temperatures up to 160°C and pressures up to 10 MPa. The bitumen sample used in this research was studied in our previous research, in which the same bitumen was not effectively diluted by *n*-butane because of the coexistence of a butane-rich liquid with a bitumen-rich liquid phase.

In this research, the liquid/liquid separation of hydrocarbons was not observed for *n*-hexane/bitumen (HB) and *n*-octane/bitumen (OB) mixtures for the range of temperatures and pressures tested, even at solvent concentrations higher than 90 mol%. This observation indicates that the amount of solvent available near the edge of a steam chamber is expected to be entirely used for bitumen dilution beyond the chamber edge in coinjection of steam with heavier hydrocarbon solvents, such as *n*-hexane and *n*-octane.

Experiments for asphaltene precipitation at atmospheric pressure showed a larger amount of precipitates with *n*-hexane than with *n*-octane at a given solvent concentration higher than 50 wt%. For solvent concentrations less than 50 wt%, no asphaltene precipitation was observed for both solvents with the bitumen sample tested in this research.

Introduction

Bitumen is one of the main petroleum resources in Canada, and is highly viscous and often immobile at reservoir conditions. Several bitumen-recovery technologies (such as cyclic-steam stimulation and SAGD) have been applied for bitumen recovery by decreasing bitumen viscosity at in-situ conditions (Butler 1991).

Coinjection of a small amount of solvent with steam, such as expanding-solvent SAGD, has been proposed and pilot tested to improve the efficiency of SAGD (Nasr and Isaacs 2001; Nasr et al. 2003; Gupta and Gittins 2007). A properly designed coinjection of solvent with steam can benefit from latent heat of the injected vapor and from bitumen dilution by solvent. The incremental oil recovery of steam/solvent coinjection in comparison with steam-only injection has been presented in laboratory-scale physical experiments, pore-scale experiments, and numerical simulations (Redford and McKay 1980; Li and Mamora 2010; Mohammadzadeh et al. 2012; Jha et al. 2013). A successful coinjection of steam with solvent can reduce the energy and water consumption while improving displacement efficiency in comparison with SAGD (Ardali et al. 2012; Keshavarz et al. 2015a, b).

The efficiency of SAGD and its variants depends largely on the temperature and composition near the edge of a steam chamber at the operating pressures. Various hydrocarbons were tested as potential additives to steam. Li and Mamora (2010) noted that a successful coinjection of steam and solvent should be designed to take advantage of the solvent without losing heat of steam. They stated that *n*-hexane was a better choice for Athabasca reservoirs because of its similar boiling points with steam. Hosseininejad Mohebati et al. (2010) found that steam/hexane coinjection could improve SAGD performance for Athabasca bitumen more than for that of Cold Lake and Lloydminster reservoirs. Yazdani et al. (2011) indicated that *n*-hexane and *n*-heptane were preferable for Athabasca bitumen compared with propane and *n*-pentane. Li et al. (2011) stated that heavy liquid solvents, such as C_{12}, were the optimal solvents to be coinjected with steam for Athabasca bitumen.

Several papers reported that lighter hydrocarbon solvents were suitable for coinjection with steam. Ardali et al. (2010) simulated the coinjection of steam and normal hydrocarbons (C_{3-7}), and concluded that *n*-butane was the optimal solvent for Cold Lake with no initial solution gas at the operating pressure of 3400 kPa. Govind et al. (2008) observed a lower residual oil saturation and a higher drainage rate simulated for *n*-butane coinjection at a higher operating pressure (4000 kPa).

Gao et al. (2016) showed in their experimental study that mixtures of Athabasca bitumen with *n*-butane can exhibit complex multiphase behavior. They observed up to three equilibrium phases for a mixture of bitumen with *n*-butane between 50 and 160°C, which consist of the bitumen-rich liquid (L_1), butane-rich liquid (L_2), and vapor (V) phases. At 140.1°C, for example, the transition from a single-phase liquid to L_1L_2 occurred at 9.1 MPa, and the transition from L_1L_2 to L_1L_2V occurred at 2.9 MPa. The observed liquid/liquid separation of hydrocarbons indicates that *n*-butane may not be entirely used for diluting bitumen ahead of a steam-chamber edge, even if a high level of accumulation of *n*-butane takes place there. Also, the effect of the resulting multiphase flow on in-situ bitumen production is uncertain. The experimental results for bitumen/*n*-butane mixtures by Gao et al. (2016) have raised the question whether liquid/liquid separation of hydrocarbons occurs for heavier solvents, such as hexane and octane, with the same Athabasca bitumen. Those solvents that are less volatile than butane were concluded to be optimal for steam/solvent coinjection for Athabasca bitumen in various papers; hence, this question will be addressed as one of the main objectives in this paper.

Phase-behavior models for bitumen developed by use of experimental data were used for prediction of fluid behavior at reservoir conditions. For example, cubic equations of state (EOSs) were used by Díaz et al. (2011), Agrawal et al. (2012), and Kumar and Okuno (2016a, b). The perturbed-chain form of the statistical-association-fluid theory (PC-SAFT) was also applied for bitumen characterization (Zúñiga-Hinojosa et al. 2014; Ma et al. 2016). Panuganti et al. (2012) presented a characterization method for crude oil containing asphaltene components by use of PC-SAFT, and matched measured saturation pressures and asphaltene-onset data. A new characterization procedure was developed by Tavakkoli et al. (2013) by applying correlations of PC-SAFT parameters for cut fractions in crude oil. Several researchers successfully applied a cubic-plus-association (CPA) EOS for bitumen characterization (Li and Firoozabadi 2010; Jindrová et al. 2015; Zirrahi et al. 2015a, b). Design of solvent type and its concentration in coinjection requires a detailed understanding and reliable prediction of phase behavior for solvent/bitumen mixtures at a wide range of temperature at operating pressures (Nagarajan et al. 2006). However, it is not easy to find in the literature a

Original SPE manuscript received for review 6 September 2016. Revised manuscript received for review 26 November 2016. Paper (SPE 186097) peer approved 6 March 2017.

Hydrocarbons	Mass (%)
Saturates	28.6
Aromatics	30.7
Resins I	20.8
Resins II	1.8
Asphaltene	18.0

Table 1—SARA test results for Athabasca-bitumen sample. This is the same bitumen as the one studied by Gao et al. (2016).

comprehensive set of pressure/volume/temperature (PVT) data for phase behavior (or phase boundaries), density, and viscosity for the same bitumen sample with different solvents.

Zou et al. (2007) presented multiphase behavior data for Athabasca vacuum bottoms/*n*-pentane and Athabasca vacuum bottoms/*n*-heptane mixtures up to 350°C. The denser hydrocarbon-liquid phase in their study was presented to be rich in asphaltene component, as shown in the saturates/aromatics/resins/asphaltenes (SARA) test results. Agrawal et al. (2012) measured the saturation pressure for bitumen+11 wt% pentane and bitumen+30 wt% pentane at 90 to 180°C. Argüelles-Vivas et al. (2012) reported the density and viscosity data for Athabasca-bitumen/pentane mixtures with different solvent weight fractions (5.1, 10.3, and 15.4 wt%) up to 210°C and 1 MPa. Many papers presented experimental results for density and viscosity for Athabasca bitumens with *n*-pentane, *n*-hexane, *n*-heptane, and *n*-decane (Nourozieh et al. 2013, 2014, 2015a, b, d; Kariznovi et al. 2013, 2014b).

Asphlatenes are the heaviest and most polarizable fraction of crude oil, which may cause deposition problems in production wells (Vargas et al. 2009). The amounts of asphaltene precipitation and water-in-oil emulsion because of the asphaltene/water interaction are also important for selection of an optimum solvent for steam/solvent coinjection (Hascakir 2016). Previous authors reported asphaltene precipitation for solvent-diluted bitumen (Rassamdana et al. 1996; Alboudwarej et al. 2003; Buenrostro-Gonzalez et al. 2004; Sabbagh et al. 2006).

Viscosity data for bitumen and its mixtures with solvent are also essential for in-situ processes and pipeline transportation. Numerous studies for bitumen viscosity were reported in the literature (Hosseininejad Mohebati et al. 2012). Mehrotra and Svrcek (1985a, b, c; 1988) and Svrcek and Mehrotra (1989) presented the viscosity data of different Alberta bitumens at atmospheric pressure. Mehrotra and Svrcek (1986, 1987) reported the viscosity of Athabasca and Cold Lake bitumens at pressures up to 10 MPa and temperatures up to 120°C. Kariznovi et al. (2014a) and Nourozieh et al. (2015c) presented viscosity data for Athabasca bitumen up to 200°C and 10 MPa. Besides experimental studies, various researchers presented correlations for bitumen viscosity (Mehrotra and Svrcek 1986, 1987; Naseri et al. 2005; Satyro and Yarranton 2010).

This research is part of a comprehensive study of phase behavior for different solvents with an Athabasca bitumen, for which Gao et al. (2016) presented results for *n*-butane/Athabasca-bitumen/water mixtures. Water was considered as part of the components primarily because water solubility in oil affects oil-phase mobility at operating temperatures of SAGD and its variants (Glandt and Chapman 1995; Luo and Barrufet 2005; Venkatramani and Okuno 2016), and secondly because complex interactions of water with bitumen components are not fully understood (Tavakkoli et al. 2016). There are two main objectives in this research. One is to address the question about the potential liquid/liquid separation for mixtures of Athabasca bitumen with *n*-hexane and *n*-octane. The same bitumen sample as the one in Gao et al. (2016) is used for a fair comparison among *n*-butane, *n*-hexane, and *n*-octane. The other objective is to present a new set of experimental data for mixtures of Athabasca bitumen with *n*-hexane and *n*-octane, such as phase boundaries, densities, viscosities, and asphaltene precipitation.

The next section describes the experimental setup and procedure adopted in this research. The Results and Discussions section

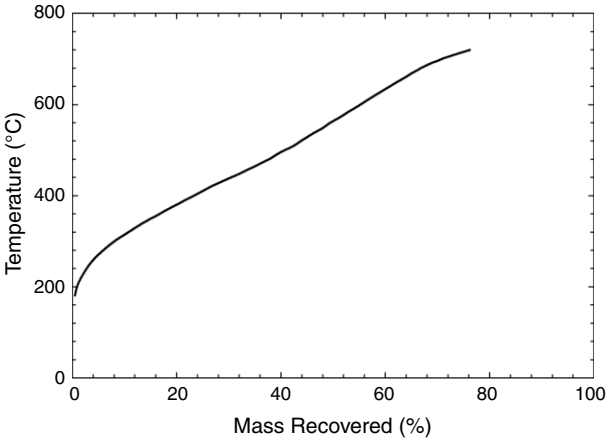

Fig. 1—Simulated-distillation-test results of the Athabasca-bitumen sample at temperatures up to 720°C.

shows experimental results and correlations for the data by use of the Peng-Robinson (PR) EOS (Peng and Robinson 1976; Robinson and Peng 1978) and other equations. To our knowledge, this is the first time PVT data are reported for *n*-octane/Athabasca-bitumen mixtures, including saturation pressures and densities at pressures up to 10 MPa and temperatures up to 160°C. A new set of PVT data is also presented for *n*-hexane/Athabasca-bitumen mixtures. Limited data for viscosity and asphaltene-precipitation measurement at atmospheric pressure are reported for *n*-hexane/Athabasca-bitumen and *n*-octane/Athabasca-bitumen mixtures.

Experimental

Materials. The same Athabasca bitumen as our previous study (Gao et al. 2016) was used for this paper. The molecular weight (MW) for the Athabasca bitumen dependent on the freezing-point depression measurement is 635 g/mol. The water content was measured to be 0.245 wt% and calculated to be 8.64 mol% in the bitumen sample, although the calculation is subject to various uncertainties, such as the bitumen MW. Removal of water from the bitumen sample by heating was not attempted to prevent light components from being evaporated. The SARA analysis results are presented in **Table 1,** for which Resins I were eluted from the column with methyl ethyl ketone and Resins II were then eluted from the column with tetrahydrofuran. The simulated distillation test was also conducted for the bitumen sample. The boiling-point distribution is shown in **Fig. 1** and **Table 2.** The resulting carbon-number distribution in mass fraction is given in **Table 3.** The solvents used are *n*-hexane and *n*-octane. The purity of *n*-hexane is 99.9% and that of *n*-octane is 99.0% (Fisher Scientific, Edmonton, Canada).

Experimental Setup. A Saybolt viscometer (K21410, Koehler, Holtsville, New York, USA) was used to measure the viscosity of the Athabasca-bitumen sample at atmospheric pressure. The temperature of the Saybolt viscometer was controlled by an oil bath with a control accuracy of ±0.03°C. The Furol orifice was factory calibrated by viscosity standard S600 at 50°C. As presented in *ASTM D88-07* (2013) for Saybolt-viscometer measurement, the repeatability is 1% by the same operator and the same apparatus.

The viscosity of the bitumen sample was also measured by use of a cone-and-plate viscometer (DV2TRV, Brookfield, Massachusetts, USA) at atmospheric pressure. The temperature of the cone-and-plate viscometer was controlled by oil or water bath with accuracy of ±1.0°C. The viscosity-measurement accuracy is ± 1.0% of a full-scale viscosity range at the corresponding rotational speed. The cone-and-plate viscometer was also used for the viscosity measurement for HB and OB mixtures at atmospheric pressure. A full-scale viscosity range (in centipoise) is calculated as the product of the torque constant *TK,* spindle-multiplier constant *SMC,* and 10,000/rev/min, where *TK* is unity for viscometer

Mass Recovered (%)	T (°C)	T (°F)	Mass Recovered (%)	T (°C)	T (°F)
0.5	181.0	357.8	39	489.3	912.7
1	203.4	398.1	40	495.9	924.6
2	226.4	439.5	41	501.6	934.9
3	244.3	471.7	42	506.8	944.2
4	258.6	497.5	43	513.7	956.7
5	270.3	518.5	44	521.4	970.5
6	280.7	537.3	45	528.6	983.5
7	290.3	554.5	46	535.8	996.4
8	299.2	570.6	47	542.2	1,008.0
9	307.1	584.8	48	548.6	1,019.5
10	314.2	597.6	49	556.8	1,034.2
11	321.6	610.9	50	563.9	1,047.0
12	328.9	624.0	51	570.2	1,058.4
13	336.1	637.0	52	577.3	1,071.1
14	343.0	649.4	53	584.7	1,084.5
15	349.4	660.9	54	591.4	1,096.5
16	355.4	671.7	55	598.4	1,109.1
17	361.9	683.4	56	605.8	1,122.4
18	368.4	695.1	57	613.1	1,135.6
19	374.4	705.9	58	620.2	1,148.4
20	380.3	716.5	59	627.1	1,160.8
21	386.4	727.5	60	634.1	1,173.4
22	392.4	738.3	61	640.9	1,185.6
23	398.2	748.8	62	648.0	1,198.4
24	404.3	759.7	63	654.4	1,209.9
25	410.4	770.7	64	661.2	1,222.2
26	416.6	781.9	65	668.4	1,235.1
27	422.5	792.5	66	674.7	1,246.5
28	427.7	801.9	67	681.2	1,258.2
29	432.9	811.2	68	686.7	1,268.1
30	438.0	820.4	69	692.0	1,277.6
31	443.0	829.4	70	696.1	1,285.0
32	448.1	838.6	71	701.1	1,294.0
33	453.8	848.8	72	704.9	1,300.8
34	459.3	858.7	73	708.7	1,307.7
35	464.5	868.1	74	712.3	1,314.1
36	470.4	878.7	75	715.8	1,320.4
37	476.2	889.2	76	719.3	1,326.7
38	481.9	899.4	76.2	720.0	1,328.0

Table 2—Simulated-distillation-test results of the Athabasca-bitumen sample at temperatures up to 720°C. This is the same bitumen as the one studied by Gao et al. (2016).

model DV2TRV and *SMC* is 9.922 for spindle CPA-52Z and 0.327 for spindle CPA-40Z.

Phase-behavior measurements for *n*-hexane/Athabasca-bitumen and *n*-octane/Athabasca-bitumen mixtures were conducted with a conventional PVT apparatus (PVT-ZS-16-2-2-H/AC, DBR, Edmonton, Canada). **Fig. 2** shows a schematic for the apparatus. Details of the PVT apparatus were presented in Gao et al. (2016). The PVT system consists of a PVT cell, an air bath, a high-pressure positive-displacement pump, and a cathetometer. The operation limits of the PVT cell are approximately 100 MPa (15,000 psi) and 199°C. The accuracy of the temperature and pressure control of the PVT system are ±0.1°C and ±0.07 MPa (10.5 psig), respectively. In addition, a high-pressure precision-test gauge (700RG31, Fluke, Calgary) with an accuracy of ±0.007 MPa (1.0 psig) was also connected to the PVT cell for more-accurate pressure measurements. The uncertainty in volume measurement is ±0.016 cm^3. The dead volume of this PVT system is 1.754 cm^3.

A digital densitometer (DDM 2910, Rudolph Research Analytical, Hackettstown, New Jersey, USA) was used to measure the reference density for bitumen/solvent mixtures at atmospheric pressure. The accuracy of temperature control is ±0.05°C. The uncertainty of the density measurement by use of this densitometer is ±0.1 kg/m^3.

Hydrocarbons	Mass Fraction	Hydrocarbons	Mass Fraction	Hydrocarbons	Mass Fraction	Hydrocarbons	Mass Fraction
C_1	<0.0001	C_{26}	0.0178	C_{51}	0.0064	C_{76}	0.0040
C_2	<0.0001	C_{27}	0.0166	C_{52}	0.0064	C_{77}	0.0045
C_3	<0.0001	C_{28}	0.0174	C_{53}	0.0059	C_{78}	0.0041
C_4	<0.0001	C_{29}	0.0179	C_{54}	0.0059	C_{79}	0.0042
C_5	<0.0001	C_{30}	0.0177	C_{55}	0.0058	C_{80}	0.0042
C_6	<0.0001	C_{31}	0.0155	C_{56}	0.0054	C_{81}	0.0047
C_7	0.0001	C_{32}	0.0154	C_{57}	0.0054	C_{82}	0.0042
C_8	0.0004	C_{33}	0.0130	C_{58}	0.0053	C_{83}	0.0043
C_9	0.0012	C_{34}	0.0128	C_{59}	0.0053	C_{84}	0.0048
C_{10}	0.0023	C_{35}	0.0110	C_{60}	0.0049	C_{85}	0.0044
C_{11}	0.0040	C_{36}	0.0107	C_{61}	0.0049	C_{86}	0.005
C_{12}	0.0068	C_{37}	0.0121	C_{62}	0.0049	C_{87}	0.0046
C_{13}	0.0101	C_{38}	0.0118	C_{63}	0.0049	C_{88}	0.0047
C_{14}	0.0115	C_{39}	0.0085	C_{64}	0.0044	C_{89}	0.0053
C_{15}	0.0146	C_{40}	0.0083	C_{65}	0.0049	C_{90}	0.0048
C_{16}	0.0156	C_{41}	0.0081	C_{66}	0.0045	C_{91}	0.0050
C_{17}	0.0171	C_{42}	0.0080	C_{67}	0.0045	C_{92}	0.0056
C_{18}	0.0190	C_{43}	0.0093	C_{68}	0.0045	C_{93}	0.0051
C_{19}	0.0190	C_{44}	0.0086	C_{69}	0.0041	C_{94}	0.0053
C_{20}	0.0201	C_{45}	0.0070	C_{70}	0.0041	C_{95}	0.0054
C_{21}	0.0195	C_{46}	0.0069	C_{71}	0.0041	C_{96}	0.0055
C_{22}	0.0201	C_{47}	0.0068	C_{72}	0.0046	C_{97}	0.0056
C_{23}	0.0184	C_{48}	0.0071	C_{73}	0.0043	C_{98}	0.0057
C_{24}	0.0182	C_{49}	0.0070	C_{74}	0.0039	C_{99}	0.0058
C_{25}	0.0171	C_{50}	0.0065	C_{75}	0.0043	C_{100+}	0.2427

Table 3—Carbon-number distribution up to C_{100} for the Athabasca-bitumen sample obtained through simulated distillation test.

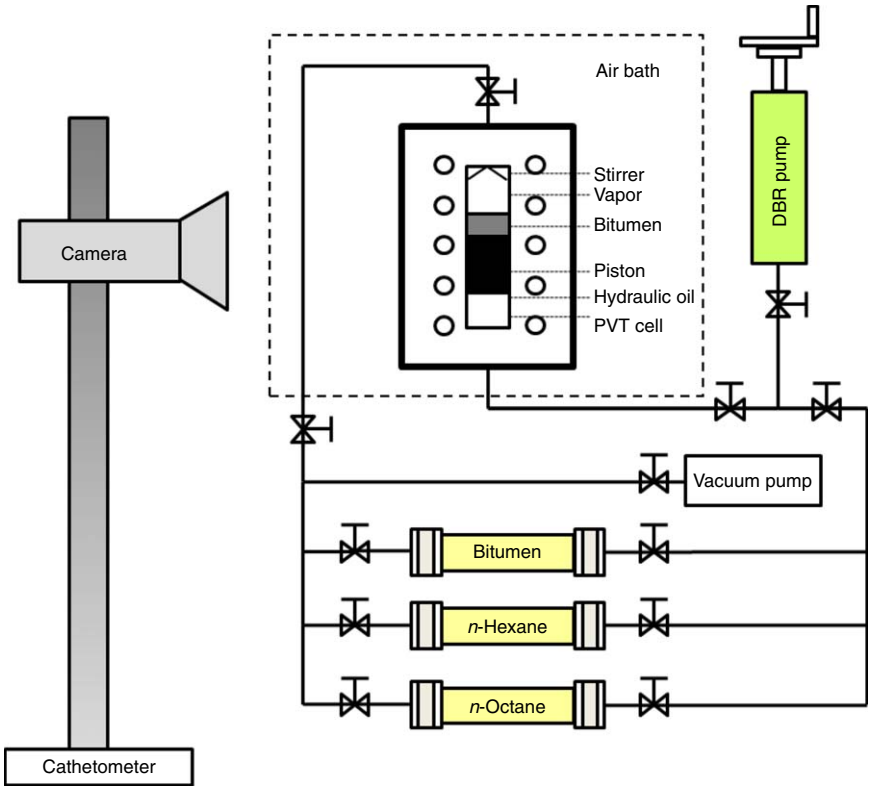

Fig. 2—Schematic of the phase-behavior experimental setup.

Mixtures	Solvent (mol%)	Dead Bitumen (mol%)	Water in Bitumen (mol%)	Solvent (wt%)	Dead Bitumen (wt%)	Water in Bitumen (wt%)	Measurement
HB1	88.27	10.72	1.01	52.67	47.21	0.13	PVT
HB2	97.53	2.26	0.21	85.38	14.59	0.04	PVT
HB3	27.50	66.24	6.26	5.31	94.44	0.25	Viscosity
HB4	44.47	50.74	4.79	10.58	89.18	0.24	Viscosity
HB5	53.81	42.21	3.99	14.69	85.08	0.23	Viscosity
HB6	81.83	16.60	1.57	39.97	59.87	0.16	Asphaltene precipitation
HB7	87.12	11.76	1.11	50.01	49.86	0.13	Asphaltene precipitation
HB8	90.40	8.77	0.83	58.20	41.69	0.11	Asphaltene precipitation
HB9	93.68	5.78	0.55	68.66	31.26	0.08	Asphaltene precipitation
HB10	96.15	3.51	0.33	78.71	21.24	0.06	Asphaltene precipitation
HB11	98.39	1.48	0.14	90.01	9.96	0.03	Asphaltene precipitation
OB1	93.71	5.75	0.54	74.49	25.45	0.07	PVT
OB2	17.35	75.52	7.13	3.95	95.79	0.26	Viscosity
OB3	36.08	58.40	5.52	9.96	89.80	0.24	Viscosity
OB4	45.84	49.49	4.67	14.23	85.55	0.23	Viscosity
OB5	77.46	20.60	1.95	40.24	59.60	0.16	Asphaltene precipitation
OB6	83.67	14.92	1.41	50.10	49.76	0.13	Asphaltene precipitation
OB7	88.48	10.53	0.99	60.07	39.82	0.11	Asphaltene precipitation
OB8	92.25	7.08	0.67	69.99	29.93	0.08	Asphaltene precipitation
OB9	95.34	4.26	0.40	80.04	19.91	0.05	Asphaltene precipitation
OB10	97.87	1.95	0.18	90.00	9.97	0.03	Asphaltene precipitation

Table 4—Compositions and measurement type for the mixtures discussed in this research. The bitumen sample used in this study is dead bitumen containing a small amount of water. Removal of water from the bitumen sample by heating was not attempted to prevent light components from being evaporated.

Experimental Procedure

Experiments were conducted for viscosities with the two viscometers, saturation pressures and densities with the PVT system, and asphaltene precipitation by following *ASTM D4124-09* (2009). In all, 21 mixtures were created for the HB and OB systems, which are labeled as HB1 through HB11 and OB1 through OB10 **(Table 4).**

Viscosities of the bitumen were first measured by the Saybolt viscometer at atmospheric pressure over the temperature range from 60.0 to 140.0°C. The viscosity measurement was conducted by following *ASTM D88-07* (2013). After setting the oil bath to a test temperature, the bitumen sample was strained into the viscometer until the fluid level was above the overflow rim. A sufficient time was needed for reaching thermal equilibrium. An equilibrium state was deemed to be achieved once the reading of thermometer became steady. Then, the cork was snapped simultaneously with the timer. The corrected efflux time in seconds (i.e., the Saybolt Furol viscosity) for 60 cm^3 of sample through the calibrated Furol orifice was measured at different temperatures. The dynamic viscosity of the bitumen sample was calculated with the following equations:

$$\mu_{SUS} = 10\mu_{SFS}, \quad \ldots\ldots\ldots\ldots\ldots\ldots\ldots\ldots\ldots (1)$$

$$\text{when } \mu_{SUS} < 100, \quad \gamma = 0.226\mu_{SUS} - 195/\mu_{SUS}, \quad \ldots\ldots (2)$$

$$\text{when } \mu_{SUS} > 100, \quad \gamma = 0.220\mu_{SUS} - 135/\mu_{SUS}, \quad \ldots\ldots (3)$$

$$\mu = \gamma\rho, \quad \ldots\ldots\ldots\ldots\ldots\ldots\ldots\ldots\ldots\ldots (4)$$

where μ_{SFS} is the Saybolt Furol viscosity (seconds), μ_{SUS} is the Saybolt Universal viscosity (in seconds), γ is the kinematic viscosity (cs), μ is the dynamic viscosity (cp), and ρ is density (g/cm^3).

Viscosities of the bitumen sample at atmospheric pressure were also measured by use of the cone-and-plate viscometer at temperatures from 25.0 to 100.0°C. The fitted spindle (CPA-52Z) was used with the consideration of the predicted viscosity range of bitumen sample. After setting the rotational speed, the results of viscosity, toque, shear stress, shear rate, and accuracy of viscosity measurement were recorded at each test temperature. The measurement was repeated twice at the same temperature because of the large uncertainty in viscosity measurement for highly viscous fluids. The viscosities of the HB mixtures (Mixtures HB3, HB4, and HB5) and the OB mixtures (Mixtures OB3 and OB4) were also measured by following the same procedure with the cone-and-plate viscometer with the CPA-40Z spindle. The CPA-52Z spindle was used for Mixture OB2 to avoid exceeding the operating limit of the CPA-40Z spindle, which is 32,700 cp.

Saturation-pressure measurements were conducted by use of the constant-composition-expansion-test method with the PVT system. Before each measurement, the PVT cell and inlet tubings were cleaned with toluene and evacuated with a vacuum pump. For the measurement of each mixture, sufficient amounts of bitumen and solvent were separately injected into two transfer cylinders that were directly connected to the inlet tubing of the PVT cell. Then, the transfer cylinders were placed in the air bath, which was set to 50.0°C for at least 12 hours. After reaching thermal equilibrium, the solvent was first injected into the PVT cell. The injected mass of solvent was calculated by use of the volume measured by the cathetometer and density values from the National Institute of Standards and Technology (NIST) database (Lemmon et al. 2016). The bitumen sample was then injected into the PVT cell without turning on the magnetic stirrer. After injection, the volume of bitumen was determined as the difference between the total volume and the solvent volume because no volume change upon mixing was assumed to occur for a short time period. The composition of this mixture was calculated by use of the densities, volumes, and MWs of bitumen and solvent. After that, the temperature of the PVT cell was increased to the highest operating temperature in this research, 160.0°C, for facilitating the mixing of bitumen and solvent. Subsequently, the mixture was vigorously stirred with the magnetic stirrer at 160.0°C for at least 12 hours. During the mixing, the injected bitumen gradually

T (°C)	μ_{SFS} (seconds)	μ (cp)
60.0	998.3	2,158.4
65.0	697.8	1,504.0
70.0	488.8	1,050.2
75.0	350.2	750.0
80.0	257.5	549.7
85.0	189.5	403.2
90.0	142.5	302.0
95.0	113.6	240.1
100.0	93.1	195.9
105.0	74.9	157.0
110.0	63.9	133.5
115.0	54.5	113.3
120.0	40.6	84.0
125.0	34.4	70.9
130.0	30.3	62.0
135.0	26.5	54.1
140.0	22.1	44.7

Table 5—Saybolt Furol viscosities (μ_{SFS}) measured by use of the Saybolt viscometer and dynamic viscosities (μ) calculated from 60.0 to 140.0°C at atmospheric pressure. Dynamic viscosities of bitumen were determined by use of the Saybolt Furol viscosity and the calculated bitumen densities by use of the correlated Tait equation in Gao et al. (2016).

moved downward as the orientation of the PVT cell was switched to the inverted position. The counterflow of bitumen and solvent occurred under the operation of the magnetic stirrer, which enabled the components to be well-mixed.

At each temperature, saturation-pressure measurements of bitumen/solvent systems were started from a single-liquid-phase state at a high pressure. Then, the pressure was gradually decreased by stepwise expansion at the rate of 3 cm^3/hr, while the mixture was sufficiently stirred for quickly reaching an equilibrium state. Mixing by the stirrer was observed as circular movement for the fluid inside the PVT cell. After reaching each specified pressure, the magnetic stirrer was switched off and the system was kept static for a sufficient duration. An equilibrium state was deemed to be achieved once the cell pressure became steady; 2 to 3 hours were sufficient for a single liquid phase to reach an equilibrium state at each temperature/pressure condition. The time allowed for equilibration was increased to 4 to 5 hours for multiphase equilibrium. Thereafter, the phase-equilibrium state of the mixture was visually identified, and the volume of each phase was measured. Then, a saturation pressure was calculated by plotting the total volume with respect to pressure, and was determined as the intersection of two pressure/volume lines because the pressure/volume relationship often showed a clear change in slope when the vapor phase appeared as pressure changed, as shown in Appendix A.

The densities of HB and OB mixtures were measured with the PVT cell dependent on mass balance at conditions of 50.0 to 160.0°C and 1.0 to 10.0 MPa. Because the mass injected into the closed PVT cell was conserved, the densities at different temperature/pressure conditions were obtained by use of the reference density that was measured at a known reference condition:

$$\rho_2 = \frac{V_1}{V_2}\rho_1 = \frac{H_1}{H_2}\rho_1, \quad \ldots\ldots\ldots\ldots\ldots\ldots\ldots\ldots\ldots (5)$$

where ρ_1, V_1, and H_1 are the sample density (kg/m^3), volume (cm^3), and height in the PVT cell (cm) at the reference conditions, respectively. ρ_2, V_2, and H_2 are the sample density (kg/m^3), volume (cm^3), and height in the PVT cell (cm) at a given temperature/pressure condition. The reference densities of mixtures were measured with the digital densitometer (DDM 2910, Rudolph Research Analytical).

The asphaltene-precipitation measurements were conducted for HB and OB mixtures following *ASTM D4124-09* (2009) at 20.4°C and atmospheric pressure. Different amounts of solvents were mixed with 30 g of bitumen to make the solvent-mass fractions used in this study, which are approximately 0.4, 0.5, 0.6, 0.7, 0.8, and 0.9. The mass of bitumen and solvent were measured by an electronic balance (MXX 412, Denver Instrument, Bohemia, New York, USA). After a mixture was prepared, it was first mixed by a glass rod. After that, a magnetic stir (6795-220, Corning, New York, USA) was used for sufficient mixing for 10 hours. Thereafter, the mixture was left for 10 hours for precipitation. Then, the diluted bitumen was filtered by use of a vacuum system with 0.25-μm-pore-size filter paper (Grade 5 Whatman filter paper, GE Healthcare Life Sciences, Chicago). Afterward, the precipitated asphaltene was dried in an oven at a temperature higher than the solvent's boiling point for 10 hours (heating temperature for HB mixtures is 116.0°C and for OB mixtures is 152.2°C). The weight of the dried asphaltene after heating was recorded.

Results and Discussions

Bitumen. **Table 5** gives the measured Saybolt Furol viscosities and the calculated dynamic viscosities for bitumen sample at atmospheric pressure from 60.0 to 140.0°C. Dynamic viscosities of bitumen were determined by Saybolt Furol viscosity and bitumen density calculated by use of the correlated Tait equation presented in Gao et al. (2016). As expected, the viscosity of the bitumen sample decreased with increasing temperature at atmospheric pressure, and the effect of temperature on bitumen viscosity is more significant at lower temperatures.

Viscosities of the bitumen sample at atmospheric pressure were also measured by the cone-and-plate viscometer at temperatures from 25.0 to 100.0°C. The measurement was repeated twice by use of the same spindle and at similar rotational speeds. The deviations of measured viscosity data at corresponding temperatures are within the uncertainty of measurement. The results of viscosity, torque, shear stress, shear rate, and accuracy of measurement were recorded as shown in **Table 6.**

Measured viscosities at atmospheric pressure were correlated with the correlation developed by Khan et al. (1984):

$$\ln(\mu) = \exp[b_1 + b_2 \ln(T + 273.15)], \quad \ldots\ldots\ldots\ldots\ldots (6)$$

in which μ is bitumen viscosity at atmospheric pressure (cp), T is temperature (°C), and b_1 and b_2 are the fitting parameters. **Table 7** gives the fitting parameters for the viscosity data measured by the Saybolt viscometer, with which the average absolute relative deviation (AARD) is 3.9%. The fitting parameters of Eq. 6 for the viscosity data measured by the cone-and-plate viscometer were compared with those for the Saybolt viscometer, as summarized in Table 7. **Fig. 3** indicates that the correlation can represent the experimental data.

The bitumen sample (with 0.245 wt% of water) was characterized by the use of the PR EOS with the van der Waals mixing rules (Peng and Robinson 1976; Robinson and Peng 1978). For consistency, it was aimed to obtain a single set of parameters for the PR EOS to correlate all data obtained in this paper for *n*-hexane/bitumen/water and *n*-octane/bitumen/water and in Gao et al. (2016) for *n*-butane/bitumen/water. Water was included in the EOS model because modeling of the solubility of water in oil is important in numerical simulation of SAGD and its variants (Venkatramani and Okuno 2016) and because bubblepoints of the bitumen are determined largely by the vapor pressures of water at corresponding temperatures (Gao et al. 2016). The PR EOS was used in this research mainly because it was shown to give reasonable predictions in terms of water solubility in oil (Venkatramani and Okuno 2015).

The bitumen was split into four pseudocomponents (PCs) by use of the chi-squared distribution (Quiñones-Cisneros et al. 2004) with the degree of freedom of 4.0. Gao et al. (2016)

First Measurement						
T (°C)	Speed (rev/min)	Torque (%)	Shear Stress (dynes/cm^2)	Shear Rate (1/seconds)	μ (cp)	Accuracy (cp)
25.0	1	98.2	1949	2	97,430	992.2
30.0	2	99.4	1972	4	49,310	496.1
40.0	6	89	1766	12	14,720	165.4
50.0	18	93.4	1853	36	5,148	55.12
60.0	40	85.2	1691	80	2,113	24.81
70.0	100	98	1945	200	972.4	9.92
80.0	180	90.8	1802	360	500.5	5.51
90.0	200	56.6	1123	400	280.8	4.96
100.0	200	34.4	682.6	400	170.7	4.96
Second Measurement						
T (°C)	Speed (rev/min)	Torque (%)	Shear Stress (dynes/cm^2)	Shear Rate (1/seconds)	μ (cp)	Accuracy (cp)
25.0	0.9	91	1806	1.8	100,300	1,102
30.0	1.8	92	1826	3.6	50,710	551.2
40.0	6	90.2	1790	12	14,920	165.4
50.0	18	95.3	1891	36	5,253	55.12
60.0	40	86.5	1717	80	2,146	24.81
70.0	90	88.9	1764	180	980.1	11.02
80.0	180	91.6	1818	360	504.9	5.51
90.0	200	57.6	1143	400	285.8	4.96
100.0	200	36	714.4	400	178.6	4.96

Table 6—Measured bitumen viscosities from 25.0 to 100.0°C at atmospheric pressures by use of the cone-and-plate viscometer. After setting the rotational speed at each test temperature, the torque, shear stress, shear rate, viscosity, and accuracy were recorded from the viscometer. The accuracy is 1.0% of the full-scale viscosity range at the corresponding rotational speed.

Coefficients	Saybolt Viscometer	Cone and Plate Viscometer, Measurement 1	Cone and Plate Viscometer, Measurement 2
b_1	21.5036	23.3463	23.4760
b_2	–3.3511	–3.6691	–3.6914
AARD (%)	3.9	2.7	3.6

Table 7—The fitting parameters for the correlation equation (Eq. 6) (Khan et al. 1984) for bitumen viscosities at atmospheric pressure measured with the Saybolt viscometer and the cone-and-plate viscometer.

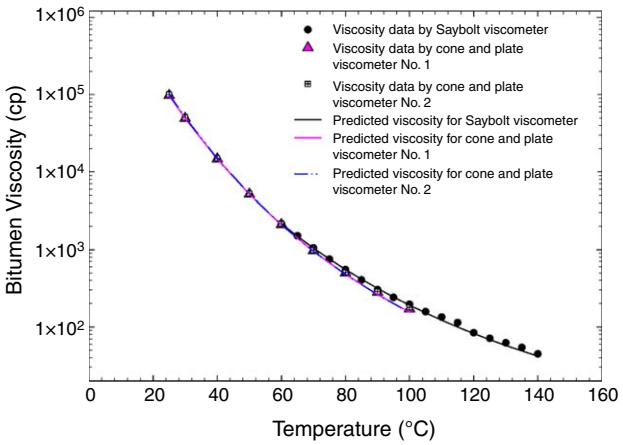

Fig. 3—The comparison between the correlated bitumen viscosity and experimental data measured by the Saybolt viscometer and the cone-and-plate viscometer. The predicted viscosities were calculated with Eq. 6 at corresponding temperatures with the fitting parameters presented in Table 7.

presented details of the procedure used to characterize the bitumen, which determined properties of PCs and binary-interaction parameters (BIPs) of water with PCs **(Tables 8 and 9).** Therefore, the PC properties and BIPs of water with PCs given in Tables 8 and 9 are the same as those used in Gao et al. (2016).

The BIPs of water with *n*-hexane and *n*-octane (Table 9) are derived from Venkatramani and Okuno (2015). The BIPs of *n*-alkanes with PCs were first calculated with the correlations used in Mehra (1981) and Li (1983) with the constant $n = 1$:

$$k_{ij} = 1 - \left(\frac{2\sqrt{V_{C_i}^{1/3} V_{C_j}^{1/3}}}{V_{C_i}^{1/3} + V_{C_j}^{1/3}} \right)^n, \quad \ldots\ldots\ldots\ldots\ldots\ldots\ldots (7)$$

where V_{C_i} and V_{C_j} are the critical volumes for components (cm^3/mol). Then, these BIPs were adjusted for matching measured saturation/pressure data for mixtures HB1 and OB1. Volume-shift parameters (C_{PEN}) were determined by reducing the overall deviation in terms of liquid density by use of data from Gao et al. (2016) and the current paper.

As shown in the next subsections and Gao et al. (2016), a comprehensive set of phase-behavior data was obtained for a number of mixtures of the same bitumen with different alkane solvents

	MW	T_c (°C)	P_c (MPa)	ω	V_c (cm^3/mol)	C_{PEN} (cm^3/mol)	Bitumen (mol%)
C_6	86.176	234.5	3.025	0.3010	368.570	–3.111	0.00
C_8	114.230	295.6	2.492	0.3980	485.407	3.879	0.00
Water	18.010	373.9	22.064	0.3433	63.071	–0.091	8.64
PC-1	296.939	435.0	2.146	0.8423	612.873	–147.701	48.84
PC-2	662.802	495.1	1.507	0.9429	920.536	–275.005	21.88
PC-3	1082.668	725.0	1.364	1.0225	1,299.294	–447.976	13.40
PC-4	2003.494	1072.9	1.045	1.1486	2,192.365	–936.360	7.24

Table 8—Components' properties of the characterized EOS model and the bitumen-sample composition. Bitumen was characterized as a mixture of four PCs: PC-1, PC-2, PC-3, and PC-4. C_{PEN} is the volume-shift parameter of Péneloux and Rauzy (1982).

	C_6	C_8	Water	PC-1	PC-2	PC-3
C_8	0.0000	–	–	–	–	–
Water	0.5790	0.5270	–	–	–	–
PC-1	0.0036	0.0008	0.2006	–	–	–
PC-2	0.0115	0.0057	0.1694	0.0000	–	–
PC-3	0.0217	0.0133	0.1694	0.0000	0.0000	–
PC-4	0.0426	0.0308	0.1694	0.0000	0.0000	0.0000

Table 9—BIPs used for the EOS model.

(*n*-butane, *n*-hexane, and *n*-octane) at temperatures up to 160°C and pressures up to 10 MPa. The studied mixtures exhibited complex phase behavior associated with the polar interaction of water with bitumen components, such as asphaltenes, in the presence of *n*-alkane solvents at high concentrations. Representation of such phase behavior was found to be difficult with the PR EOS with the van der Waals mixing rules (Gao 2016), and will be studied by use of more-sophisticated thermodynamic models in the future.

In general, a cubic EOS is limited in correlative accuracy for mixtures of molecules with large differences in size (Panuganti et al. 2012). EOS parameters for asphaltene components are also highly uncertain. Tavakkoli et al. (2016) presented that asphaltenes in Athabasca bitumen were highly attracted to the oil/water interface, both before and after the detection of asphaltene precipitation. The research by Tavakkoli et al. (2016) indicated that interactions between water and asphaltene components should be considered for modeling of bitumen/solvent/water mixtures. The Athabasca-bitumen sample used in this study contained 0.245 wt% of water and 18.0 wt% of asphaltene components. The self and cross-association energy for water and asphaltenes are not considered in the current EOS model, and may have caused the deviations between predictions and measured data in this paper (discussed in the following subsections) and Gao et al. (2016).

HB Mixtures. Saturation pressures were measured for Mixture HB1 at temperatures from 80.8 to 159.6°C to address whether liquid/liquid separation occurs for this Athabasca bitumen with *n*-hexane. Only single-liquid-phase and liquid/vapor-phase (LV) equilibria were observed through the PVT-cell window within this temperature range at less than 10 MPa. The total volume and

T (°C)	Pressure (MPa)	Volume Fraction of Liquid Phase	Volume Fraction of Vapor Phase
80.8	0.177	0.899	0.101
80.8	0.170	0.868	0.132
80.8	0.170	0.840	0.160
111.1	0.412	0.957	0.043
111.1	0.405	0.920	0.080
111.1	0.405	0.896	0.104
111.1	0.398	0.869	0.131
111.1	0.398	0.836	0.164
140.8	0.846	0.951	0.049
140.8	0.839	0.918	0.082
140.8	0.832	0.881	0.119
140.8	0.818	0.852	0.148
159.6	1.232	0.955	0.045
159.6	1.218	0.929	0.071
159.6	1.191	0.890	0.110
159.6	1.177	0.857	0.143
159.6	1.163	0.819	0.181

Table 10—Measured liquid-phase and vapor-phase volume fractions for Mixture HB1 at different temperature/pressure conditions.

	Experimental Data		Predictions From EOS Model	
T (°C)	Pressure (MPa)	ρ^{sat} (kg/m^3)	Pressure (MPa)	ρ^{sat} (kg/m^3)
80.8	0.209	845.0	0.178	747.2
111.1	0.426	813.0	0.423	719.6
140.8	0.880	784.4	0.715	690.6
159.6	1.290	754.5	0.974	669.6

Table 11—Measured and predicted saturation pressures and densities at saturation points of Mixture HB1. Only single-liquid-phase and liquid/vapor-phase equilibria were observed within this temperature range for Mixture HB1.

volume of each phase were recorded by use of a cathetometer. **Table 10** shows the variation of liquid-phase and vapor-phase volume fractions measured at different pressures for Mixture HB1 (Table 4). **Table 11** summarizes the results and the comparison with predictions from the EOS model (Tables 8 and 9). The bubblepoints were observed at higher pressures than *n*-hexane's vapor pressures at the test temperatures, and were reasonably correlated by the EOS model, as shown in **Fig. 4.** The AARD is 15% for the bubblepoints (i.e., boundaries for the presence of the vapor phase). The EOS model predicts a separate water (W) phase at less than 108.0°C. Such a phase was not observed in the PVT experiment, although water may have precipitated as invisible water-in-oil emulsion in the bulk oil phase.

A further PVT experiment was conducted for Mixture HB2. This mixture has a higher solvent concentration of 97.53 mol%, which is close to the butane concentration, 97.24 mol%, for the butane/bitumen mixture (Mixture B) studied by Gao et al. (2016). However, only L and LV equilibria were observed at less than 10 MPa at 159.8°C. The bubblepoint pressure was 1.238 MPa at 159.8°C. **Fig. 5** shows the digital images of a single-liquid phase at 4.199 MPa and LV two phases at 0.931 MPa at 159.8°C for Mixture HB2. No further experiments were conducted at lower temperatures for Mixture HB2 because of the limited availability of the PVT system for this research. It seems unlikely that liquid/liquid separation occurs for this Athabasca bitumen with *n*-hexane at lower temperatures because the level of miscibility between the two liquid phases, if present, would increase at lower temperatures (Gao 2016).

By use of the procedure mentioned in the Experimental section, densities of Mixture HB1 were measured at different temperature/pressure conditions by use of the PVT cell, as summarized in **Table 12.** The reference density was measured at 51.1°C and atmospheric pressure by the densitometer.

Densities measured for Mixture HB1 were first compared with the values calculated with Eq. 8, assuming no volume change on mixing:

$$\frac{1}{\rho_m} = \frac{w_s}{\rho_s} + \frac{1 - w_s}{\rho_B}, \quad \ldots\ldots\ldots\ldots\ldots\ldots\ldots\ldots \quad (8)$$

where ρ_m is the mass density of the solvent/bitumen mixture; w_s is the weight fraction of solvent; and ρ_s and ρ_B are the mass densities of solvent and bitumen, respectively. The values for ρ_s at different conditions were obtained from the NIST database (Lemmon et al. 2016). The ρ_B values were calculated from the correlated Tait equation presented in Gao et al. (2016). The resulting AARD is 13%, which indicates that volume change on mixing should be considered for Mixture HB1. Therefore, an excess-volume mixing rule,

$$\frac{1}{\rho_m} = \frac{w_s}{\rho_s} + \frac{1 - w_s}{\rho_B} - w_s(1 - w_s)\left(\frac{1}{\rho_s} + \frac{1}{\rho_B}\right)\gamma, \quad \ldots\ldots\ldots \quad (9)$$

was used to correlate the data. In Eq. 9, γ is the parameter between solvent and bitumen for this model. The best-fitted γ, 0.2520, was

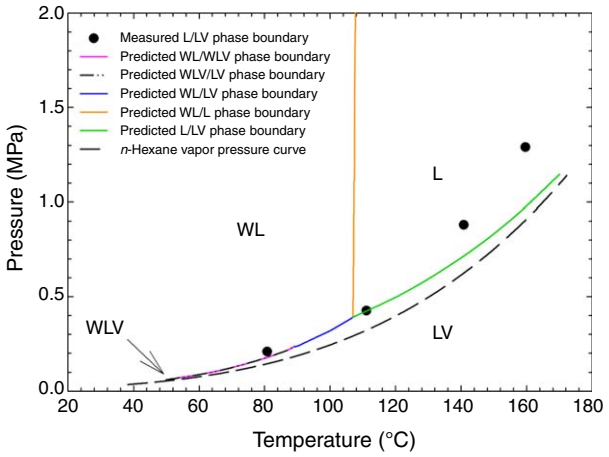

Fig. 4—Measured and predicted saturation pressures for Mixture HB1 at different temperatures. The vapor-phase composition is calculated to be nearly 100% *n*-hexane. L = oleic phase; W = aqueous phase; V = vapor phase.

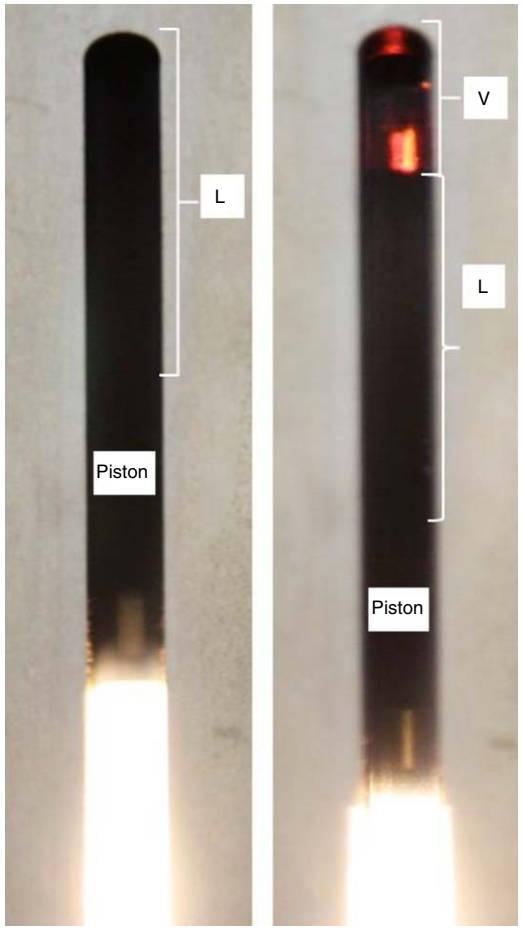

Fig. 5—Digital images captured for Mixture HB2: (a) single-liquid-phase equilibrium at 159.8°C and 4.199 MPa; (b) LV equilibrium at 159.8°C and 0.931 MPa.

T (°C)	Pressure (MPa)	ρ (kg/m^3)	T (°C)	Pressure (MPa)	ρ (kg/m^3)
51.1	1.122	878.6	111.1	7.093	828.6
51.1	4.093	884.2	111.1	10.133	834.3
51.1	7.093	889.3	140.8	1.101	783.9
51.1	10.133	892.6	140.8	4.107	790.9
80.8	1.129	846.9	140.8	7.113	796.6
80.8	4.128	853.4	140.8	10.133	801.7
80.8	7.113	859.5	159.6	4.114	760.2
80.8	10.140	865.1	159.6	7.100	766.6
111.1	1.136	814.8	159.6	10.126	772.7
111.1	4.128	820.9	–	–	–

Table 12—Densities of Mixture HB1 measured at different temperature/pressure conditions by the PVT cell by use of constant composition expansion.

obtained by regression to the measured densities (Table 12). It gives the AARD of 0.3%, which is much lower than that from Eq. 8. The predicted densities by use of the EOS model give an AARD of 12% with respect to the experimental data (Table 12).

Viscosities of HB mixtures (Mixtures HB3, HB4, and HB5 given in Table 4) at atmospheric pressure were measured by use of the cone-and-plate viscometer at temperatures from 25.0°C to 90.0°C, as shown in **Table 13.**

Mixture HB3						
T (°C)	Speed (rev/min)	Torque (%)	Shear Stress (dynes/cm^2)	Shear Rate (1/seconds)	μ (cp)	Accuracy (cp)
25	0.3	96.8	237.4	2.25	10,550	109
30	0.4	80.4	197.2	3	6,573	81.75
40	1.1	88	215.8	8.25	2,616	29.73
50	2.5	91.2	223.7	18.75	1,193	13.08
60	4.5	82.7	202.8	33.75	601	7.27
70	8.5	84.9	208.2	63.75	326.6	3.85
80	15	89	218.3	112.5	194	2.18
90	25	91.7	224.9	187.5	119.9	1.31
Mixture HB4						
T (°C)	Speed (rev/min)	Torque (%)	Shear Stress (dynes/cm^2)	Shear Rate (1/seconds)	μ (cp)	Accuracy (cp)
25	1.4	88.7	217.5	10.5	2,072	23.36
30	1.9	83.7	205.3	14.25	1,441	17.21
40	3.7	84.3	206.7	27.75	745	8.84
50	7	88.9	204.8	48.75	415.3	5.03
60	11	84.5	207.2	82.5	251.2	2.97
70	17	81.5	199.9	127.5	156.8	1.92
80	28	87.8	215.3	210	102.5	1.17
90	40	94.3	231.3	300	77.09	0.82
Mixture HB5						
T (°C)	Speed (rev/min)	Torque (%)	Shear Stress (dynes/cm^2)	Shear Rate (1/seconds)	μ (cp)	Accuracy (cp)
25	3.2	88.1	216.1	24	900.3	10.22
30	4.2	85	208.5	31.5	661.8	7.79
40	8	89.6	219.7	60	366.2	4.09
50	12	81.6	200.1	90	222.4	2.73
60	20	86.6	212.4	150	141.6	1.64
70	28	84.3	206.7	210	98.45	1.17
80	40	82.1	201.4	300	67.12	0.82
90	55	91.4	224.2	412.5	54.34	0.59

Table 13—Viscosities of HB mixtures, HB3, HB4, and HB5, given in Table 4, measured at different temperatures and atmospheric pressure by use of the cone-and-plate viscometer.

Model	AARD (mol%)	AARD (wt%)	AARD (vol%)
Arrhenius	81.77	397.17	190.81
Cragoe	97.65	24.75	47.20
Power-law	46.20 (n = 0.1002)	7.67 (n = –0.1885)	15.01 (n = –0.1321)
Lederer	–	–	37.75 (θ = 0.4072)

Table 14—Calculated AARDs of different models for prediction and correlation of the viscosities measured for HB mixtures (HB3, HB4, and HB5 given in Table 4). Nourozieh et al. (2015b) presented for Athabasca-bitumen/*n*-hexane mixtures that the coefficients for the power law with mole fraction, weight fraction, and volume fraction were 0.0186, –0.3365, and –0.2049, respectively. They also presented the coefficient for the Lederer correlation to be 0.2869 in their research.

Mixtures	$M_{bitumen}$ (g)	$M_{solvent}$ (g)	Solvent Weight Fraction	$M_{asphaltene}$ (g)	Fractional Yield
HB6	30.230	20.125	0.3997	0	0.0000
HB7	29.425	29.433	0.5001	0	0.0000
HB8	29.970	41.720	0.5820	2.168	0.0723
HB9	29.920	65.540	0.6866	3.204	0.1071
HB10	29.885	110.455	0.7871	4.279	0.1432
HB11	29.550	266.223	0.9001	4.944	0.1673

Table 15—Results of asphaltene-precipitation measurements for HB mixtures HB6, HB7, HB8, HB9, HB10, and HB11 given in Table 2.

Centeno et al. (2011) summarized a total of 26 mixing rules. Viscosities measured for HB mixtures were evaluated with four models—Arrhenius, Cragoe, power law, and Lederer—used for heavy-oil/solvent mixtures by Nourozieh et al. (2015a, b). These equations are given next.

$$\text{Arrhenius:}\quad \mu_m = \mu_s^{x_s} \times \mu_B^{(1-x_s)}, \quad \ldots\ldots\ldots\ldots\ldots\ldots (10)$$

where μ_m is the viscosity of a solvent/bitumen mixture, x_s is the mole fraction of solvent, and μ_s and μ_B are the viscosities of solvent and bitumen, respectively.

$$\text{Cragoe:}\quad \frac{1}{\ln(2000\mu_m)} = \frac{w_s}{\ln(2000\mu_s)} + \frac{1-w_s}{\ln(2000\mu_B)}, \quad \ldots\ldots (11)$$

where w_s is the weight fraction of solvent.

$$\text{Power law:}\quad \mu_m = [x_s\mu_s^n + (1-x_s)\mu_B^n]^{1/n}, \quad \ldots\ldots\ldots (12)$$

where n is the adjustable parameter in this model, and should be obtained through regression for a minimum AARD.

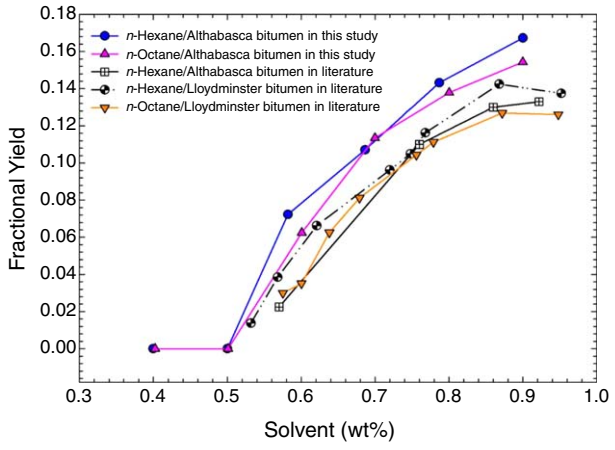

Fig. 6—Comparison of measured asphaltene-precipitation data with the data by Alboudwarej et al. (2003).

$$\text{Lederer:}\ \ln\mu_m = \left(1 - \frac{\theta\phi_B}{\theta\phi_B + \phi_s}\right)\ln\mu_s + \left(\frac{\theta\phi_B}{\theta\phi_B + \phi_s}\right)\ln\mu_B, \quad \ldots\ldots\ldots\ldots\ldots\ldots (13)$$

where θ is the adjustable parameter between 0.0 and 1.0 in this model, and should be obtained through regression for a minimum AARD. ϕ_s is the volume fraction of solvent.

Following the research by Nourozieh et al. (2015b), the fraction of solvent was considered as mole, weight, and volume fractions for Eqs. 10, 11, and 12. Then, the total AARDs were calculated for all data for Mixtures HB3, HB4, and HB5, as shown in **Table 14.** Table 14 also shows the values for n and θ used for Eqs. 12 and 13 in this paper. Results show that the power-law model with weight fraction results in a more-accurate correlation than the other models for Mixtures HB3, HB4, and HB5. The power-law model with volume fraction gave the best results for HB mixtures in Nourozieh et al. (2015b).

Asphaltene-precipitation measurements were conducted at ambient conditions for bitumen diluted with *n*-hexane (Mixtures HB6, HB7, HB8, HB9, HB10, and HB11, given in Table 4). The measured asphaltene-precipitation fractional yields are shown in **Table 15. Fig. 6** presents the fractional yields obtained in this research, along with the data presented in the literature (Alboudwarej et al. 2003). The Athabasca bitumen used in this study yielded more asphaltene than the other bitumens because of the higher asphaltene content (Table 1) compared with 14.6 wt% asphaltene content for Athabasca bitumen and 15.1 wt% for Lloydminster bitumen in Alboudwarej et al. (2003). No precipitated asphaltene was observed for the concentrations of *n*-hexane, 39.97 wt% (83.10 mol%) and 50.01 wt% (88.08 mol%), at 20.4°C and atmospheric pressure in this research.

The results shown in Table 15 indicate that asphaltene precipitation may have occurred in the PVT experiment for Mixture HB2, considering the high *n*-hexane concentration. Asphaltene precipitates may have resided in the oleic phase as dispersed particles, as described in Agrawal et al. (2012). However, it was not possible to observe asphaltene precipitation with the current PVT setup, which is not equipped with a solid-detection unit.

OB Mixtures. Saturation pressures of Mixture OB1 were measured at 140.7 and 159.0°C. Only single-liquid-phase and

T (°C)	Pressure (MPa)	Volume Fraction of Liquid Phase	Volume Fraction of Vapor Phase
140.7	0.156	0.883	0.117
140.7	0.150	0.867	0.133
140.7	0.143	0.845	0.155
159.0	0.219	0.876	0.124
159.0	0.212	0.865	0.135
159.0	0.205	0.853	0.147
159.0	0.191	0.797	0.203

Table 16—Measured liquid-phase and vapor-phase volume fractions for Mixture OB1 at different temperature/pressure conditions.

	Experimental Data		Predictions From EOS Model	
T (°C)	Pressure (MPa)	ρ^{sat} (kg/m^3)	Pressure (MPa)	ρ^{sat} (kg/m^3)
140.7	0.198	687.7	0.227	669.0
159.0	0.247	673.0	0.311	650.7

Table 17—Measured and predicted saturation pressures and densities at saturation points of Mixture OB1. Only single-liquid-phase and liquid/vapor-phase equilibria were observed within this temperature range for Mixture OB1.

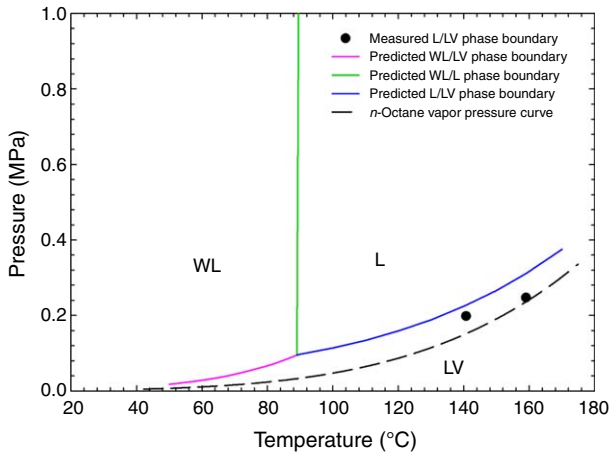

Fig. 7—Measured and predicted saturation pressure of Mixture OB1 at different temperatures. The vapor-phase composition is calculated to be nearly 100% *n*-octane.

liquid/vapor-phase equilibria were observed through the PVT-cell window within this temperature range. It was challenging to measure saturation pressures at lower temperatures because they are close to or less than atmospheric pressure. **Table 16** shows the variation of liquid-phase and vapor-phase volume fractions measured at different pressures for Mixture OB1. **Table 17** summarizes the results and the comparison with predictions from the EOS model (Tables 8 and 9). The EOS model reasonably correlates the data, as shown in **Fig. 7.** The AARD is 20% for the bubblepoints. As in the subsection HB Mixtures, the water phase predicted at less than 90.0°C by the EOS model was not observed in the PVT experiment. However, it is possible that water droplets have resided as water-in-oil emulsion in the bulk-oil phase below a temperature limit of water-in-oil solubility.

The densities of Mixture OB1 were measured at different temperature/pressure conditions by use of the PVT cell, as summarized in **Table 18.** The reference density was measured at 50.2°C and atmospheric pressure by the densitometer (subsection Experimental Setup). Thereafter, measured densities for Mixture OB1 were compared with the calculated values by use of Eqs. 8 and 9. The AARD is 3.5% with Eq. 8 and 0.2% with Eq. 9. The best-fitted γ for Eq. 9 is 0.0966 for Mixture OB1. The predicted densities by use of the EOS model give an AARD of 2.7% compared with experimental data (Table 18).

Viscosities of OB mixtures (Mixtures OB2, OB3, and OB4 given in Table 4) at atmospheric pressure were also measured by use of the cone-and-plate viscometer from 25.0 to 90.0°C, as shown in **Table 19.** Measured viscosities of OB mixtures were also compared with Eqs. 10, 11, 12, and 13. The total AARDs for Mixtures OB2, OB3, and OB4 with Eqs. 11 through

T (°C)	Pressure (MPa)	ρ (kg/m^3)	T (°C)	Pressure (MPa)	ρ (kg/m^3)
50.2	1.101	768.4	110.5	7.100	727.0
50.2	4.107	772.2	110.5	10.113	731.5
50.2	7.106	775.5	140.7	1.094	690.0
50.2	10.092	779.6	140.7	4.100	694.0
80.2	1.101	744.1	140.7	7.100	699.8
80.2	4.114	747.8	140.7	10.099	705.1
80.2	7.106	751.7	159.0	1.101	674.3
80.2	10.119	756.5	159.0	4.100	678.6
110.5	1.094	718.5	159.0	7.100	682.5
110.5	4.100	721.5	159.0	10.099	686.8

Table 18—Densities of Mixture OB1 measured at different temperature/pressure conditions by the PVT cell by use of constant-composition expansion.

Mixture OB2						
T (°C)	Speed (rev/min)	Torque (%)	Shear Stress (dynes/cm^2)	Shear Rate (1/seconds)	μ (cp)	Accuracy (cp)
25	7	86.5	1717	14	12,260	141.7
30	12	90	1786	24	7,441	82.68
40	30	91.4	1814	60	3,023	33.07
50	60	82.3	1633	120	1,361	16.54
60	130	86.6	1718	260	661	7.63
70	200	71.8	1425	400	356.2	4.96
80	200	43.4	861.2	400	215.3	4.96
90	200	28.1	557.6	400	139.4	4.96
Mixture OB3						
T (°C)	Speed (rev/min)	Torque (%)	Shear Stress (dynes/cm^2)	Shear Rate (1/seconds)	μ (cp)	Accuracy (cp)
25	0.6	92.2	226.1	4.5	5,025	54.5
30	0.9	90.4	221.7	6.75	3,285	36.33
40	2	85.4	209.4	15	1,396	16.35
50	4	84.4	207	30	690	8.18
60	8	90.8	222.7	60	371.1	4.09
70	14	93.8	230	105	219.1	2.34
80	20	85.1	208.7	150	139.1	1.64
90	30	85.1	208.7	225	92.76	1.09
Mixture OB4						
T (°C)	Speed (rev/min)	Torque (%)	Shear Stress (dynes/cm^2)	Shear Rate (1/seconds)	μ (cp)	Accuracy (cp)
25	2.5	82.8	203.1	18.75	1,083	13.08
30	3.5	85.5	209.7	26.25	798.8	9.34
40	6	88.5	217	45	482.3	5.45
50	10	88.5	217	75	289.4	3.27
60	17	94.4	231.5	127.5	181.6	1.92
70	25	93	228.1	187.5	121.6	1.31
80	37	90	220.7	277.5	79.54	0.88
90	50	89.5	219.5	375	58.53	0.65

Table 19—Viscosities of OB mixtures measured at different temperatures and atmospheric pressure by use of the cone-and-plate viscometer.

13 are presented in **Table 20.** For Mixtures OB2, OB3, and OB4, the best-fitted model is the power-law correlation with weight fraction.

Asphaltene-precipitation measurements were also conducted at ambient condition for Mixtures OB5, OB6, OB7, OB8, OB9, and OB10, given in Table 4. **Table 21** showed the measured asphaltene-precipitation fractional yields. No precipitated asphaltene was observed for the concentrations of *n*-octane, 40.24 wt% (78.95 mol%) and 50.10 wt% (84.83 mol%), at 20.4°C and atmospheric pressure. Fig. 6 showed a lower fractional yield for OB mixtures compared with *n*-hexane-diluted-bitumen, which is consistent with data presented in the literature (Rassamdana et al. 1996; Akbarzadeh et al. 2005).

Conclusions

This paper presented an experimental study of phase equilibrium, viscosity, density, and asphaltene precipitation for 11 mixtures of Athabasca bitumen with *n*-hexane and 10 mixtures of the same bitumen with *n*-octane. The bitumen sample used in this research is the same as the one used in our previous research (Gao et al. 2016) for multiphase behavior of bitumen/*n*-butane mixtures. One

Model	AARD (mol%)	AARD (wt%)	AARD (vol%)
Arrhenius	58.07	310.21	176.49
Cragoe	91.93	37.29	36.50
Power-law	55.33 (n = 0.0093)	29.17 (n = –0.2292)	34.25 (n = –0.1812)
Lederer	–	–	54.55 (θ = 0.2973)

Table 20—Calculated AARDs of different models for prediction and correlation of the viscosities measured for OB mixtures OB2, OB3, and OB4.

Mixtures	$M_{bitumen}$ (g)	$M_{solvent}$ (g)	Solvent Weight Fraction	$M_{asphaltene}$ (g)	Fractional Yield
OB5	29.680	19.985	0.4024	0.000	0.0000
OB6	30.115	30.240	0.5010	0.000	0.0000
OB7	30.070	45.240	0.6007	1.878	0.0625
OB8	29.890	69.720	0.6999	3.394	0.1135
OB9	29.470	118.160	0.8004	4.064	0.1379
OB10	29.610	266.480	0.9000	4.569	0.1543

Table 21—Asphaltene-precipitation measurement results for OB mixtures OB5, OB6, OB7, OB8, OB9, and OB10.

of the main questions addressed in this study is whether liquid/liquid separation of hydrocarbons occurs for mixtures of Athabasca bitumen with *n*-hexane or *n*-octane at conditions relevant to steam/solvent coinjection. Our conclusions are as follows:

1. The liquid/liquid immiscibility of hydrocarbons was not observed for HB and OB mixtures for the range of temperatures and pressures in this research, even at solvent concentrations greater than 90 mol%. This is in contrast to the previous research by Gao et al. (2016), in which the same bitumen was not effectively diluted by *n*-butane because of the coexistence of a butane-rich liquid with a bitumen-rich liquid phase. In coinjection of steam with heavier hydrocarbon solvents, such as *n*-hexane and *n*-octane, the amount of solvent available near the edge of a steam chamber is expected to be entirely used for diluting bitumen ahead of the edge.
2. In asphaltene-precipitation experiments at atmospheric pressure, a larger amount of precipitates was observed with *n*-hexane than with *n*-octane at a given solvent concentration greater than 50 wt%. At solvent concentrations lower than 50 wt%, no asphaltene precipitation was observed for both solvents with the Athabasca-bitumen sample used in this research.
3. The viscosity data obtained for HB and OB mixtures in this research were reasonably correlated by the power-law correlation with weight fraction. Representation of the density data obtained for HB and OB mixtures requires the excess-volume mixing rule.
4. The PR EOS (Peng and Robinson 1976; Robinson and Peng 1978) with the van der Waals mixing rules showed limited accuracy in representation of the multiphase-behavior data obtained in this paper and Gao et al. (2016) when it was used with a single set of parameters to represent all the data. Potential reasons for the limitation include polar interactions of water with bitumen components, such as asphaltenes, in the presence of *n*-alkane solvents at high concentrations. More-sophisticated EOS and/or mixing rules are expected to represent the presented data more accurately.

Nomenclature

C_{PEN} = Péneloux and Rauzy (1982) volume-shift parameter
P_c = critical pressure
T_c = critical temperature
V_c = critical volume
w_s = solvent weight fraction
x_s = solvent mole fraction
μ = viscosity
μ_{SFS} = Saybolt Furol viscosity
μ_{SUS} = Saybolt Universal viscosity
ρ = density
ϕ_s = solvent volume fraction
ω = acentric factor

Acknowledgments

Research grants from Japan Petroleum Exploration Company Limited and Japan Canada Oil Sands Limited through the Center for Petroleum and Geosystems Engineering at the University of Texas at Austin and the Natural Sciences and Engineering Research Council of Canada (RGPIN 418226 and RGPIN 05394) are gratefully acknowledged. We thank Francisco Javier Argüelles-Vivas for technical suggestions, and Todd Kinnee for his assistance in the PVT experiments at the University of Alberta.

References

Agrawal, P., Schoeggl, F. F., Satyro, M. A. et al. 2012. Measurement and Modeling of the Phase Behavior of Solvent Diluted Bitumens. *Fluid Phase Equilibr.* **334** (November): 51–64. https://doi.org/10.1016/j.fluid.2012.07.025.

Akbarzadeh, K., Alboudwarej, H., Svrcek, W. Y. et al. 2005. A Generalized Regular Solution Model for Asphaltene Precipitation From *n*-Alkane Diluted Heavy Oils and Bitumens. *Fluid Phase Equilibria* **232** (1–2): 159–170. https://doi.org/10.1016/j.fluid.2005.03.029.

Alboudwarej, H., Akbarzadeh, K., Beck, J. et al. 2003. Regular Solution Model for Asphaltene Precipitation from Bitumens and Solvents. *AIChE J.* **49** (11): 2948–2956. https://doi.org/10.1002/aic.690491124.

Ardali, M., Barrufet, M., and Mamora, D. D. 2012. Laboratory Testing of Addition of Solvents to Steam to Improve SAGD Process. Presented at SPE Heavy Oil Conference Canada, Calgary, 12–14 June. SPE-146993-MS. https://doi.org/10.2118/146993-MS.

Ardali, M., Mamora, D. D., and Barrufet, M. 2010. A Comparative Simulation Study of Addition of Solvents to Steam in SAGD Process. Presented at Canadian Unconventional Resources and International Petroleum Conference, Calgary, 19–21 October. SPE-138170-MS. https://doi.org/10.2118/138170-MS.

Argüelles-Vivas, F. J., Babadagli, T., Little, L. et al. 2012. High Temperature Density, Viscosity, and Interfacial Tension Measurements of Bitumen–Pentane–Biodiesel and Process Water Mixtures. *J. Chem. Eng. Data* **57** (10): 2878–2889. https://doi.org/10.1021/je3008217.

ASTM D88-07, Standard Test Method for Saybolt Viscosity. 2013. West Conshohocken, Pennsylvania: ASTM International. https://doi.org/10.1520/D0088.

ASTM D4124-09, Standard Test Method for Separation of Asphalt into Four Fractions. 2009. West Conshohocken, Pennsylvania: ASTM International. https://doi.org/10.1520/D4124-09.

Buenrostro-Gonzalez, E., Lira-Galeana, C., Gil-Villegas, A. et al. 2004. Asphaltene Precipitation in Crude Oils: Theory and Experiments. *AIChE J.* **50** (10): 2552–2570. https://doi.org/10.1002/aic.10243.

Butler, R.M. 1991. *Thermal Recovery of Oil and Bitumen*. Upper Saddle River, New Jersey: Prentice Hall.

Centeno, G., Sánchez-Reyna, G., Ancheyta, J. et al. 2011. Testing Various Mixing Rules for Calculation of Viscosity of Petroleum Blends. *Fuel* **90** (12): 3561–3570. https://doi.org/10.1016/j.fuel.2011.02.028.

Díaz, O. C., Modaresghazani, J., Satyro, M. A. et al. 2011. Modeling the Phase Behavior of Heavy Oil and Solvent Mixtures. *Fluid Phase Equilibr.* **304** (1–2): 74–85. https://doi.org/10.1016/j.fluid.2011.02.011.

Gao, J. 2016. *An Experimental Study of Multiphase Behavior for Athabasca-Bitumen/Alkane-Solvent Mixtures*. Master's thesis, University of Alberta, Edmonton, Canada.

Gao, J., Okuno, R., and Li, H. A. 2016. An Experimental Study of Multiphase Behavior for *n*-Butane/Bitumen/Water Mixtures. *SPE J.* SPE-180736-PA (in press; posted October 2016). https://doi.org/10.2118/180736-PA.

Glandt, C. A. and Chapman, W. G. 1995. The Effect of Water Dissolution on Oil Viscosity. *SPE Res Eng* **10** (1): 59–64. SPE-24631-PA. https://doi.org/10.2118/24631-PA.

Govind, P. A., Das, S. K., Srinivasan, S. et al. 2008. Expanding Solvent SAGD in Heavy Oil Reservoirs. Presented at the International Thermal Operations and Heavy Oil Symposium, Calgary, 20–23 October. SPE-117571-MS. https://doi.org/10.2118/117571-MS.

Gupta, S. C. and Gittins, S. D. 2007. Effect of Solvent Sequencing and Other Enhancements on Solvent Aided Process. *J Can Pet. Technol* **46** (9): 57–61. PETSOC-07-09-06. https://doi.org/10.2118/07-09-06.

Hascakir, B. 2016. How to Select the Right Solvent for Solvent-Aided Steam Injection Processes. *J. Pet. Sci. Eng.* **146** (October): 746–751. https://doi.org/10.1016/j.petrol.2016.07.038.

Hosseininejad Mohebati, M. H., Maini, B. B., and Harding, T. G. 2010. Optimization of Hydrocarbon Additives With Steam in SAGD for Three Major Canadian Oil Sands Deposits. Presented at Canadian Unconventional Resources and International Petroleum Conference, Calgary, 19–21 October. SPE-138151-MS. https://doi.org/10.2118/138151-MS.

Hosseininejad Mohebati, M., Maini, B. B., and Harding, T. G. 2012. Numerical-Simulation Investigation of the Effect of Heavy-Oil Viscosity on the Performance of Hydrocarbon Additives in SAGD. *SPE Res Eval & Eng* **15** (2): 165–181. SPE-138151-PA. https://doi.org/10.2118/138151-PA.

Jha, R. K., Kumar, M., Benson, I. et al. 2013. New Insights into Steam-Solvent Co-Injection Process Mechanism. *SPE J.* **18** (5): 867–877. SPE-159277-PA. https://doi.org/10.2118/159277-PA.

Jindrová, T., Mikyška, J., and Firoozabadi, A. 2015. Phase Behavior Modeling of Bitumen and Light Normal Alkanes and CO_2 by PR-EOS and CPA-EOS. *Energ. Fuel.* **30** (1): 515–525. https://doi.org/10.1021/acs.energyfuels.5b02322.

Kariznovi, M., Nourozieh, H., Guan, J. G. J. et al. 2013. Measurement and Modeling of Density and Viscosity for Mixtures of Athabasca Bitumen and Heavy *n*-alkane. *Fuel* **112** (October): 83–95. https://doi.org/10.1016/j.fuel.2013.04.071.

Kariznovi, M., Nourozieh, H., and Abedi, J. 2014a. Measurement and Correlation of Viscosity and Density for Compressed Athabasca Bitumen at Temperatures Up to 200°C. *J Can Pet Technol* **53** (6): 330–338. SPE-173182-PA. https://doi.org/10.2118/173182-PA.

Kariznovi, M., Nourozieh, H., and Abedi, J. 2014b. Volumetric Properties of Athabasca Bitumen + *n*-Hexane Mixtures. *Energ. Fuel.* **28** (12): 7418–7425. https://doi.org/10.1021/ef5019884.

Keshavarz, M., Okuno, R., and Babadagli, T. 2015a. Optimal Application Conditions for Steam/Solvent Coinjection. *SPE Res Eval & Eng* **18** (1): 20–38. SPE-165471-PA. https://doi.org/10.2118/165471-PA.

Keshavarz, M., Okuno, R., and Babadagli, T. 2015b. A Semi-Analytical Solution to Optimize Single-Component Solvent Coinjection with Steam during SAGD. *Fuel* **144** (15 March): 400–414. https://doi.org/10.1016/j.fuel.2014.12.030.

Khan, M. A. B., Mehrotra, A. K., and Svrcek, W. Y. 1984. Viscosity Models for Gas-Free Athabasca Bitumen. *J Can Pet Technol* **23** (3): 47–53. PETSOC-84-03-05. https://doi.org/10.2118/84-03-05.

Krejbjerg, K. and Pedersen, K. S. 2006. Controlling VLLE Equilibrium With a Cubic EOS in Heavy Oil Modeling. Paper presented at the Canadian International Petroleum Conference, Calgary, 13–15 June. PETSOC-2006-052. https://doi.org/10.2118/2006-052.

Kumar, A. and Okuno, R. 2016a. A New Algorithm for Multiphase Fluid Characterization for Solvent Injection. *SPE J.* **21** (5): 1688–1704. SPE-175123-PA. https://doi.org/10.2118/175123-PA.

Kumar, A. and Okuno, R. 2016b. Reliable Characterization of Bitumen Based on Perturbation from *n*-Alkanes for Steam/Solvent Coinjection Simulation. *Fuel* **182** (15 October): 141–153. https://doi.org/10.1016/j.fuel.2016.05.095.

Lemmon, E. W., McLinden, M. O., and Friend, D. G. Thermophysical Properties of Fluid System. In *NIST Chemistry WebBook*, ed. P. J. Linstrom and W. G. Mallard, National Institute of Standards and Technology, Gaithersburg, MD, http://webbook.nist.gov (retrieved 28 August 2016).

Li, Y. K. 1983. Heavy Fraction Characterization and Hypothetical Component Selection for Oil and Gas Mixtures. Computer Modelling Group Research Report R12.04, May 1983.

Li, W. and Mamora, D. D. 2010. Phase Behavior of Steam with Solvent Co-injection under Steam Assisted Gravity Drainage (SAGD) Process. Presented at SPE EUROPEC/EAGE Annual Conference and Exhibition, Barcelona, Spain, 14–17 June. SPE-130807-MS. https://doi.org/10.2118/130807-MS.

Li, W., Mamora, D. D., and Li, Y. 2011. Solvent-Type and –Ratio Impacts on Solvent-Aided SAGD Process. *SPE Res Eval & Eng* **14** (3): 320–331. SPE-130802-PA. https://doi.org/10.2118/130802-PA.

Li, Z. and Firoozabadi, A. 2010. Modeling Asphaltene Precipitation by *n*-Alkanes from Heavy Oils and Bitumens Using Cubic-Plus-Association Equation of State. *Energ. Fuel.* **24** (2): 1106–1113. https://doi.org/10.1021/ef9009857.

Luo, S. and Barrufet, M. A. 2005. Reservoir Simulation Study of Water-i*n*-Oil Solubility Effect on Oil Recovery in Steam Injection Process. *SPE Res Eval & Eng* **8** (6): 528–533. SPE-89407-PA. https://doi.org/10.2118/89407-PA.

Ma, M., Chen, S., and Abedi, J. 2016. Predicting the Multiphase Equilibrium and Density of Bitumen with C_2H_6, C_3H_8 and CO_2 Using the Simplified PC-SAFT Equation of State. *Fuel* **181** (1 October): 652–659. https://doi.org/10.1016/j.fuel.2016.05.040.

Mehra, R. K. 1981. *The Computation of Multi-Phase Equilibrium in Compositional Reservoir Studies*. PhD Dissertation, University of Calgary, Calgary.

Mehrotra, A. K. and Svrcek, W. Y. 1985a. Viscosity, Density and Gas Solubility Data for Oil Sand Bitumens. Part I: Athabasca Bitumen Saturated with CO and C_2H_6. *AOSTRA J. Res.* **1** (4): 263–268.

Mehrotra, A. K. and Svrcek, W. Y. 1985b. Viscosity, Density and Gas Solubility Data for Oil Sand Bitumens. Part II: Peace River Bitumen Saturated with N_2, CO, CH_4, CO_2 and C_2H_6. *AOSTRA J. Res.* **1** (4): 269–279.

Mehrotra, A. K. and Svrcek, W. Y. 1985c. Viscosity, Density and Gas Solubility Data for Oil Sand Bitumens. Part III: Wabasca Bitumen Saturated with N_2, CO, CH_4, CO_2 and C_2H_6. *AOSTRA J. Res.* **2** (2): 83–93.

Mehrotra, A. K. and Svrcek, W. Y. 1986. Viscosity of Compressed Athabasca Bitumen. *Can. J. Chem. Eng.* **64** (5): 844–847. https://doi.org/10.1002/cjce.5450640520.

Mehrotra, A. K. and Svrcek, W. Y. 1987. Viscosity of Compressed Cold Lake Bitumen. *Can. J. Chem. Eng.* **65** (4): 672–675. https://doi.org/10.1002/cjce.5450650423.

Mehrotra, A. K. and Svrcek, W. Y. 1988. Properties of Cold Lake Bitumen Saturated with Pure Gases and Gas Mixtures. *Can. J. Chem. Eng.* **66** (4): 656–665. https://doi.org/10.1002/cjce.5450660419.

Mohammadzadeh, O., Rezaei, N., and Chatzis, I. 2012. More Insight into the Pore-Level Physics of the Solvent-Aided SAGD (SA-SAGD) Process for Heavy Oil and Bitumen Recovery. Presented at SPE Heavy Oil Conference Canada, Calgary, 12–14 June. SPE-157776-MS. https://doi.org/10.2118/157776-MS.

Nagarajan, N. R., Honarpour, M. M., and Sampath, K. 2006. Reservoir Fluid Sampling and Characterization–Key to Efficient Reservoir Management. Presented at the Abu Dhabi International Petroleum Exhibition and Conference, Abu Dhabi, 5–8 November. SPE-101517-MS. https://doi.org/10.2118/101517-MS.

Naseri, A., Nikazar, M., and Mousavi Dehghani, S. A. 2005. A Correlation Approach for Prediction of Crude Oil Viscosities. *J. Pet. Sci. Eng.* **47** (3–4): 163–174. https://doi.org/10.1016/j.petrol.2005.03.008.

Nasr, T. N. and Isaacs, E. 2001. Process for Enhancing Hydrocarbon Mobility Using a Steam Additive. US Patent 6230814.

Nasr, T. N., Beaulieu, G., Golbeck, H. et al. 2003. Novel Expanding Solvent-SAGD Process "ES-SAGD." *J Can Pet Technol* **42** (1): 13–16. PETSOC-03-01-TN. https://doi.org/10.2118/03-01-TN.

Nourozieh, H., Kariznovi, M., Guan, J. G. et al. 2013. Measurement of Thermophysical Properties and Modeling for Pseudo-Binary Mixtures of *n*-decane and Athabasca Bitumen. *Fluid Phase Equilibr.* **347** (15 June): 62–75. https://doi.org/10.1016/j.fluid.2013.03.010.

Nourozieh, H., Kariznovi, M., and Abedi, J. 2014. Measurement and Prediction of Density for the Mixture of Athabasca Bitumen and Pentane at Temperatures up to 200°C. *Energ. Fuel.* **28** (5): 2874–2885. https://doi.org/10.1021/ef4022784.

Nourozieh, H., Kariznovi, M., and Abedi, J. 2015a. Viscosity Measurement and Modeling for Mixtures of Athabasca Bitumen/*n*-Pentane at Temperatures up to 200°C. *SPE J.* **20** (2): 226–238. SPE-170252-PA. https://doi.org/10.2118/170252-PA.

Nourozieh, H., Kariznovi, M., and Abedi, J. 2015b. Viscosity Measurement and Modeling for Mixtures of Athabasca Bitumen/Hexane. *J.*

Pet. Sci. Eng. **129** (May): 159–167. https://doi.org/10.1016/j.petrol.2015.03.002.

Nourozieh, H., Kariznovi, M., and Abedi, J. 2015c. Density and Viscosity of Athabasca Bitumen Samples at Temperatures Up to 200°C and Pressures Up to 10 MPa. *SPE Res Eval & Eng* **18** (3): 375–386. SPE-176026-PA. https://doi.org/10.2118/176026-PA.

Nourozieh, H., Kariznovi, M., and Abedi, J. 2015d. Modeling and Measurement of Thermo-Physical Properties for Athabasca Bitumen and *n*-heptane Mixtures. *Fuel* **157** (1 October): 73–81. https://doi.org/10.1016/j.fuel.2015.04.032.

Panuganti, S. R., Vargas, F. M., Gonzalez, D. L. et al. 2012. PC-SAFT Characterization of Crude Oils and Modeling of Asphaltene Phase Behavior. *Fuel* **93** (March): 658–669. https://doi.org/10.1016/j.fuel.2011.09.028.

Péneloux, A. and Rauzy, E. 1982. A Consistent Correction for Redlich-Kwong-Soave Volumes. *Fluid Phase Equilibr.* **8** (1): 7–23. https://doi.org/10.1016/0378-3812(82)80002-2.

Peng, D. Y. and Robinson, D. B. 1976. A New Two-Constant Equation of State. *Ind. Eng. Chem. Fundamen.* **15** (1): 59–64. https://doi.org/10.1021/i160057a011.

Quiñones-Cisneros, S. E., Dalberg, A., and Stenby, E. H. 2004. PVT Characterization and Viscosity Modeling and Prediction of Crude Oils. *Pet. Sci. Tech.* **22** (9–10): 1309–1325. https://doi.org/10.1081/LFT-200034092.

Rassamdana, H., Dabir, B., Nematy, M. et al. 1996. Asphalt Flocculation and Deposition: I. The Onset of Precipitation. *AIChE J.* **42** (1): 10–22. https://doi.org/10.1002/aic.690420104.

Redford, D. A. and McKay, A. S. 1980. Hydrocarbon-Steam Processes for Recovery of Bitumen from Oil Sands. Presented at SPE/DOE Enhanced Oil Recovery Symposium, Tulsa, 20–23 April. SPE-8823-MS. https://doi.org/10.2118/8823-MS.

Robinson, D. B. and Peng, D. Y. 1978. The Characterization of the Heptanes and Heavier Fractions for the GPA Peng-Robinson Programs. Research report, Gas Processors Association, Tulsa.

Sabbagh, O., Akbarzadeh, K., Badamchi-Zadeh, A. et al. 2006. Applying the PR-EoS to Asphaltene Precipitation from *N*-alkane Diluted Heavy Oils and Bitumens. *Energ. Fuel.* **20** (2): 625–634. https://doi.org/10.1021/ef0502709.

Satyro, M. A. and Yarranton, H. W. 2010. Expanded Fluid-Based Viscosity Correlation for Hydrocarbons Using an Equation of State. *Fluid Phase Equilibr.* **298** (1): 1–11. https://doi.org/10.1016/j.fluid.2010.06.023.

Svrcek, W. Y. and Mehrotra, A. K. 1989. Properties of Peace River Bitumen Saturated with Field Gas Mixtures. *J Can Pet Technol* **28** (2): 50–56. PETSOC-89-02-01. https://doi.org/10.2118/89-02-01.

Tavakkoli, M., Chen, A., Sung, C. et al. 2016. Effect of Emulsified Water on Asphaltene Instability in Crude Oils. *Energ. Fuel.* **30** (5): 3676–3686. https://doi.org/10.1021/acs.energyfuels.5b02180.

Tavakkoli, M., Panuganti, S. R., Taghikhani, V. et al. 2013. Precipitated Asphaltene Amount at High-Pressure and High-Temperature Conditions. *Energ. Fuel.* **28** (3): 1596–1610. https://doi.org/10.1021/ef401074e.

Vargas, F. M., Gonzalez, D. L., Creek, J. L. et al. 2009. Development of a General Method for Modeling Asphaltene Stability. *Energ. Fuel.* **23** (3): 1147–1154. https://doi.org/10.1021/ef800666j.

Venkatramani, A. and Okuno, R. 2015. Characterization of Water-Containing Reservoir Oil Using an EOS for Steam Injection Processes. *J. Nat. Gas Sci. Eng.* **26** (September): 1091–1106. https://doi.org/10.1016/j.jngse.2015.07.036.

Venkatramani, A. and Okuno, R. 2016. Compositional Mechanisms in Steam-Assisted Gravity Drainage and Expanding-Solvent Steam-Assisted Gravity Drainage With Consideration of Water Solubility in Oil. *SPE Res Eval & Eng* SPE-180737-PA (in press; posted September 2016).

Yazdani, A. J., Alvestad, J. A., Kjonsvik, D. et al. 2011. A Parametric Simulation Study for Solvent Co-injection Process in Bitumen Deposits. Presented at the Canadian Unconventional Resources Conference, Calgary, 15–17 November. SPE-148804-MS. https://doi.org/10.2118/148804-MS.

Zirrahi, M., Hassanzadeh, H., and Abedi, J. 2015a. Prediction of CO_2 Solubility in Bitumen Using the Cubic-Plus-Association Equation of State (CPA-EOS). *J. Supercrit. Fluid.* **98** (March): 44–49. https://doi.org/10.1016/j.supflu.2015.01.001.

Zirrahi, M., Hassanzadeh, H., and Abedi, J. 2015b. Prediction of Water Solubility in Petroleum Fractions and Heavy Crudes Using Cubic-Plus-Association Equation of State (CPA-EoS). *Fuel* **159** (1 November): 894–899. https://doi.org/10.1016/j.fuel.2015.07.058

Zou, X.-Y., Zhang, X., and Shaw, J. A. 2007. Phase Behavior of Athabasca Vacuum Bottoms + *N*-alkane Mixtures. *SPE Prod & Oper* **22** (2): 265–272. SPE-97661-PA. https://doi.org/10.2118/97661-PA.

Zúñiga-Hinojosa, M. A., Justo-García, D. N., Aquino-Olivos, M. A. et al. 2014. Modeling of Asphaltene Precipitation from *n*-Alkane Diluted Heavy Oils and Bitumens Using the PC-SAFT Equation of State. *Fluid Phase Equilibr.* **376** (25 August): 210–224. https://doi.org/10.1016/j.fluid.2014.06.004.

Appendix A—Measured PV Data for Bitumen at 80.8°C

In **Fig. A-1,** measured pressure/volume data for HB (Mixture HB1) are shown at 80.8°C. Only single-liquid-phase and liquid/vapor-phase equilibria were observed at this temperature. The saturation point is determined as the intersection of two pressure/volume lines.

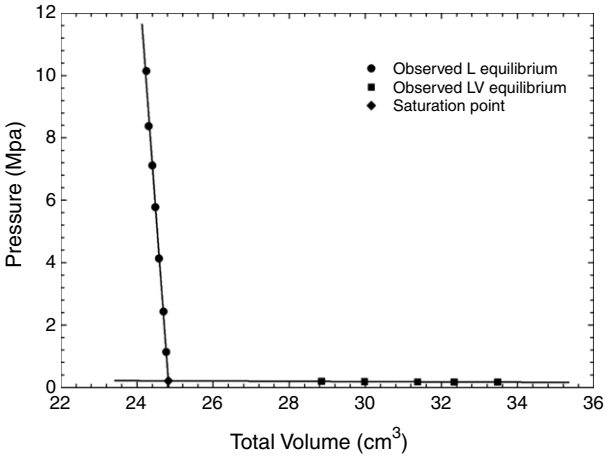

Fig. A-1—Measured PV data for bitumen at 80.8°C.

Jianyi Gao holds a bachelor's degree from the China University of Petroleum, Beijing, and a master's degree from the University of Alberta, both in petroleum engineering. Her research interests include multiphase behavior, thermodynamics, and heavy oil recovery. Gao is a member of SPE.

Ryosuke Okuno is an assistant professor in the Department of Petroleum and Geosystems Engineering at the University of Texas at Austin. Before his current position, he served as an assistant professor of petroleum engineering at the University of Alberta from 2010 to 2015. Okuno also has 7 years of industrial experience as a reservoir engineer with Japan Petroleum Exploration Company Limited, and is a registered professional engineer in Alberta, Canada. His research and teaching interests include enhanced oil recovery, heavy-oil recovery, numerical reservoir simulation, thermodynamics, multiphase behavior, and applied mathematics. Okuno is a recipient of the 2012 SPE Petroleum Engineering Junior Faculty Research Initiation Award, and holds the Pioneer Corporation Faculty Fellowship in Petroleum Engineering at the University of Texas at Austin. He is also an associate editor for *SPE Journal* and *Journal of Natural Gas Science & Engineering*. Okuno holds bachelor's and master's degrees in geosystems engineering from the University of Tokyo, and a PhD degree in petroleum engineering from the University of Texas at Austin.

Huazhou Andy Li is an assistant professor in petroleum engineering at the University of Alberta. His research interests include experimental and theoretical studies on the phase behavior of reservoir fluids, carbon dioxide enhanced oil recovery, surfactant-alternating-gas flooding, thermal and nonthermal heavy-oil recovery, stimulation of tight oil/gas

reservoirs with supercritical carbon dioxide, and production optimization of oil reservoirs by use of reservoir simulations. Li has authored or coauthored 32 peer-reviewed technical papers and has presented 16 papers in SPE conferences and other international conferences. He is a member of SPE and the American Chemical Society. Li volunteers as a technical editor for *SPE Journal* and as an associate editor for *Journal of Natural Gas Science & Engineering*. He has received the 2016 SPE Outstanding Technical Editor Award for *SPE Journal*, the 2016 Outstanding Contribution in Reviewing Award from *Fuel*, and the 2014 Outstanding Contribution in Reviewing from *Journal of Natural Gas Science & Engineering*. Li holds bachelor's and master's degrees, both in petroleum engineering, from the China University of Petroleum, East China, and a PhD degree in petroleum systems engineering from the University of Regina, Canada.